Chinese Journal of Aeronautics, (2023), xxx(xx): xxx–xxx

Chinese Society of Aeronautics and Astronautics
& Beihang University

Chinese Journal of Aeronautics

cja@buaa.edu.cn
www.sciencedirect.com

FULL LENGTH ARTICLE

Deflagration and detonation induced by shock wave focusing at different Mach numbers

Zezhong YANG, Jun CHENG, Bo ZHANG *

School of Aeronautics and Astronautics, Shanghai Jiao Tong University, Shanghai 200240, China

Received 5 February 2023; revised 27 February 2023; accepted 28 April 2023

KEYWORDS

Deflagration;
Detonation;
Hydrogen;
Ignition;
Shock wave focusing

Abstract Shock wave focusing is an effective way to create a hot spot or a high-pressure and high-temperature region at a certain place, showing its unique usage in detonation initiation, which is beneficial for the development of detonation-based engines. The flame propagation behavior after the autoignition induced by shock wave focusing is crucial to the formation and self-sustaining of the detonation wave. In this study, wedge reflectors with two different angles (60° and 90°) and a planar reflector are employed, and the Mach number of incident shock waves ranging from 2.0 to 2.8 is utilized to trigger different flame propagation modes. Dynamic pressure transducers and the high-speed schlieren imaging system are both employed to investigate the shock-shock collision and ignition procedure. The results reveal a total of four flame propagation modes: deflagration, DDT (Deflagration-to-Detonation Transition), unsteady detonation, and direct detonation. The detonation wave formed in the DDT and unsteady detonation mode is only approximately 75%−85% of the Chapman-Jouguet (C-J) speed; meanwhile, the directly induced detonation wave speed is close to the C-J speed. Transverse waves, which are strong evidence for the existence of detonation waves, are discovered in experiments. The usage of wedge reflectors significantly reduces the initial pressure difference ratio needed for direct detonation ignition. We also provide a practical method for differentiating between detonation and deflagration modes, which involves contrasting the speed of the reflected shock wave with the speed of the theoretically nonreactive reflected shock wave. These findings should serve as a reference for the detonation initiation technique in advanced detonation propulsion engines.

1. Introduction

In recent years, the application of detonation waves in hypersonic aerospace propulsion systems has been universally noticed for their higher thermodynamic efficiency and higher heat release rate.[1,2] Detonation engines such as Pulse Detonation Engines (PDEs),[3,4] Rotating Detonation Engines (RDEs),[5] and Oblique Detonation Engines (ODEs)[6,7] are all promising airbreathing hypersonic or supersonic propulsion techniques. In addition, a novel shock-focusing detonation engine configuration that used a concave reflector to ignite the detonation wave has been proposed as an improvement

* Corresponding author at: Shanghai Jiao Tong University, School of Aeronautics and Astronautics, Shanghai 200240, China.
E-mail address: bozhang@sjtu.edu.cn (B. ZHANG).

https://doi.org/10.1016/j.cja.2023.06.029

Please cite this article in press as: YANG Z et al. Deflagration and detonation induced by shock wave focusing at different Mach numbers, *Chin J Aeronaut* (2023), https://doi.org/10.1016/j.cja.2023.06.029

Nomenclature

v_{ie}	experimental incident shock wave velocity	v_{2t}	theoretical nonreactive velocity behind incident shock wave
v_{it}	theoretical incident shock wave velocity	Ma_i	Mach number of incident shock wave
v_{re}	experimental reflected shock wave velocity	p_1	initial pressure of driven section
v_{rt}	theoretical reflected shock wave velocity	p_4	initial pressure of driver section
v_{CJ}	theoretical Chapman-Jouguet detonation velocity		
v_{2e}	experimental velocity behind incident shock wave		

of PDEs in recent years.[8,9] Unlike the common Deflagration-To-Detonation Transition (DDT) conducted in an ordinary tube or tubes with obstacles[10] or jets[11] to accelerate DDT, where hot spots randomly form in unpredictable positions, the shock wave focusing technique can create a certain hot spot or region at the desired position and initiate direct detonation, showing a promising future for low-cost stable detonation initiation, which is crucial for detonation engine designs. The important role of shock wave focusing in detonation initiation can also be confirmed in various DDT processes.[12,13]

As a shock wave travels into a cavity, it will converge in the direction of propagation and produce a locally high-pressure and high-temperature region at the center of convergence. A pioneering study of shock wave focusing was conducted by Meshkov.[14] Several types of cylindrically concave reflectors were tested, and the shock wave strength was substantially enhanced in the shock wave focusing procedure. The three stages of the pressure field and the three-shock intersections in parabolic reflectors were experimentally studied by Sturtevant and Kulkarny.[15] Duong and Milton[16] investigated the shock wave converging in cones ranging from 10° to 30°. Izumi et al.[17] combined both experimental and computational methods to study the structure of the reflected shock wave after the shock-shock collision in parabolic reflectors with different depths. Lodato et al.[18] used a fifth-order high-resolution method to simulate the shock wave reflected from a shallow wavy wall. It is noteworthy that they also used a nonlinear wave equation to quantitatively analyze the movement of triple point and transverse waves. Wedge-like reflectors have been discussed by Bond,[19] Eliasson,[20] and Dimotakis[21] et al. A special type of reflector that can smoothly transform a planar shock wave into a curved shock wave was designed by Zhai[22] and Luo[23] et al. according to the Chester-Chisnell-Whitham (CCW) approximation. Liverts and Apazidis[24] found that a focal temperature on the order of 30000 K is measured in their converging-shock-wave experiments. The aforementioned nonreactive shock wave focusing experiments and simulations more or less indicate that the extremely high temperature and pressure point formed at the focus point of shock waves or region after strong interactions between the shock waves. Chan[25] first applied the shock wave focusing technique in combustible mixture ignition. The local hot spots were capable of causing strong ignition, and the blast wave could develop into a detonation wave. Gelfand et al.[26] investigated the ignition behavior in a hydrogen-air mixture, and Bartenev et al.[27] numerically studied the relationship between the Mach number of the incident shock wave and combustion mode. Zhang et al.[28,29] systematically performed a series of experiments and demonstrated the existence of several ignition modes in shock wave focusing procedures with different reflectors. Energy accumulation in the shock wave focusing process was believed to be the resource of the critical energy for ignition.[30,31] Li and Zhang[32] confirmed the energy-accumulation effect of wedge reflectors. Schlieren images showed that it is more conducive to initiate the detonation wave with a smaller angle wedge reflector at a lower speed shock wave. Yang and Zhang[33] combined both numerical and experimental methods to investigate the flame propagation modes in different angle wedge reflectors. They found that the hot spot formed in the 60° wedge reflector tends to have a higher intensity than the 90° wedge reflector, triggering a more stable detonation wave.

Although numerous studies on autoignition induced by shock wave focusing have been carried out, most of them still lack quantitative analysis of the flame evolution procedure. To the best of our knowledge, the flame velocity, which is a critical indicator of the flame mode, whether it is a deflagration wave or a detonation wave, has never been discussed in previous shock wave focusing research. Our study combines the high-speed schlieren imaging technique with pressure and OH* emission measurement systems to explore the autoignition and flame propagation procedure. A hydrogen–oxygen mixture is utilized in our shock tube experiments for its importance in the aerospace propulsion field.[5–7] For a specific case (Ma_i = 2.0, 90° wedge reflector), an additional nonreactive simulation is performed to provide a better explanation of the flow field. Furthermore, two different DDT processes are revealed. The structures of shock waves and reaction fronts with different reflectors are systematically discussed. The comparison of the velocity of the reflected shock wave and Chapman-Jouguet (C-J) speed is presented and analyzed.

2. Experimental setup

The experiment of autoignition induced by shock wave focusing is carried out in a double-diaphragm stainless steel shock tube. As shown in Fig. 1(a), the tube is composed of three parts: a 1 m-long driver section, a 1 m-long driven section, and a 0.1 m-long double diaphragm section. The inner cross-section of the tube is a 40 mm × 73 mm rectangle. Moreover, the shock tube is equipped with sidewall windows for schlieren imaging, and its size is 200 mm × 73 mm. The drive section's end wall is replaceable, where different-shaped reflectors can be installed. A planar reflector and two different-angled wedge reflectors, a 60° wedge reflector and a 90° wedge reflector, are employed in this experiment. The apex of the wedge reflector has been removed to create a 7 mm-wide plane, and a through hole is drilled in the plane's center to accommodate a piezo-

Please cite this article in press as: YANG Z et al. Deflagration and detonation induced by shock wave focusing at different Mach numbers, *Chin J Aeronaut* (2023), https://doi.org/10.1016/j.cja.2023.06.029

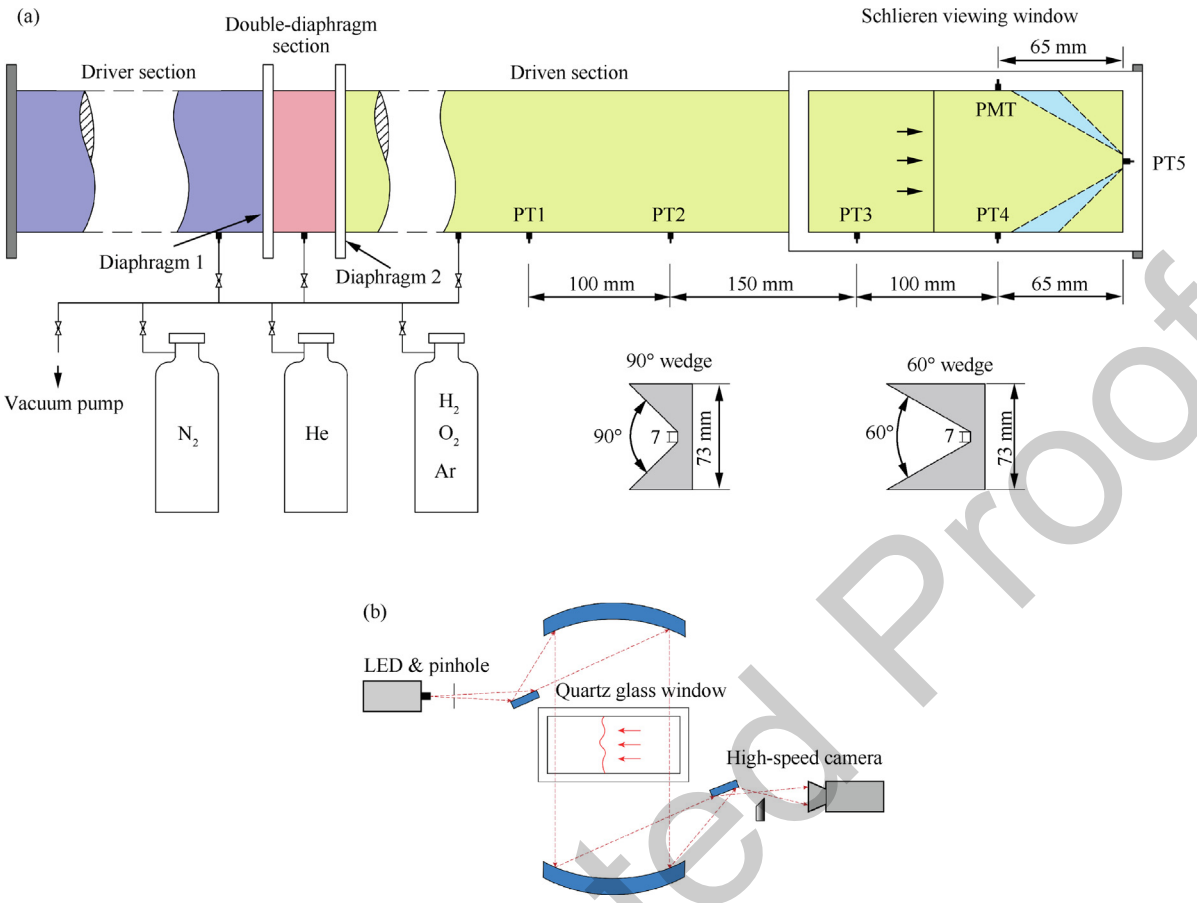

Fig. 1 Schematic diagram of (a) shock tube experimental system and (b) high-speed schlieren imaging system.

electric pressure transducer (PT5). Other pressure transducers (PT1–PT4) are mounted along the sidewall of the driven section. The spectral signal of combustion is obtained and amplified by a Photomultiplier Tube (PMT). The optical measurement window is positioned directly opposite PT4, and the emission spectrum of the OH* radicals is isolated through a 306.5 nm bandpass filter. By comparing the arrival time of the pressure spike with the OH* signal, we can easily determine the combustion state at this cross-section. PT2 and PT3 used here are PCB piezoelectric sensors (113B26), while PT1, PT4, and PT5 are Kistler piezoelectric sensors (603CBA). The signals from pressure transducers and PMT are recorded by a PicoScope 4824 with a sampling frequency of 200 kHz. A Z-type schlieren system equipped with a high-speed camera (Phantom V710L) is also utilized to capture flow field changes, as shown in Fig. 1(b). The camera has a frame rate of 150,000 frame/s and a resolution of 320 pixel × 104 pixel. The high-speed camera can shoot continuously for 3 s in this setting, which is long enough to meet the experiment's demands.

In this experiment, the driven gas is a stoichiometric hydrogen–oxygen mixture diluted with 90 vol% argon, and it is premixed in a 40 L chamber for at least 24 h. Helium is chosen to be the driver gas because it is the lightest inert gas, promising a higher Mach number for the incident shock wave. After the three sections of the tube are all vacuumed to a pressure below 0.1 kPa, the driven gas and the driver gas are filled into the corresponding section at specific pressures, which are shown in Table 1. Meanwhile, the double-diaphragm section is filled with driver gas at half the pressure between the two adjacent sections. When all preparations are finished, the solenoid valve on the double-diaphragm section opens, and the pressure imbalance ruptures the diaphragms, generating an incident shock wave with the desired intensity.

3. Results and discussion

3.1. Validation of experimental results

First, the accuracy of the experimental results has been validated. Cases 1–5 (Table 1) were tested with all three different reflectors. Extra cases that have not been shown in Table 1 are conducted with a planar reflector to verify the agreement between the experiment and calculation (Fig. 2(a)). The velocity of the incident shock wave is obtained by comparing the location difference of the shock wave. At least 15 schlieren images are used in the shock-wave velocity calculation to ensure the accuracy of the calculation. For nonreactive shock-tube experiments, as long as we know the Mach number of the incident shock wave (Ma_i) and the initial gas state of the driver section and the driven section, we can obtain all the flow properties in the tube according to the Rankine-Hugoniot relation. Because the gas after the incident shock wave has not been ignited in all experimental cases, the shock wave incident process can be considered inert, which means it is also suitable for the aforementioned theoretical calculation.

Table 1 Initial gas conditions for Cases 1–5.

Case	Ma_i	Driver section	Driven section	p_4/p_1
		p_4(kPa)	p_1(kPa)	
1	2.0	550	60.36	9.11
2	2.2	550	44.01	12.50
3	2.4	550	32.73	16.80
4	2.6	550	24.72	22.25
5	2.8	550	18.91	29.09

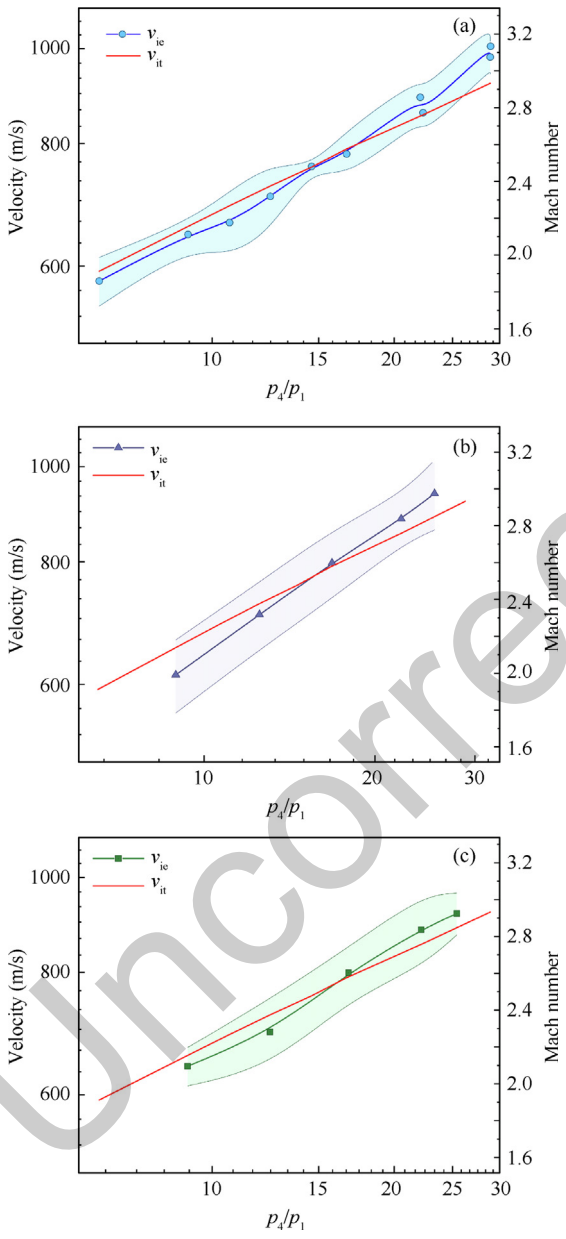

Fig. 2 Comparison between experimental results and theoretical results: (a) Planar reflector, (b) 60° wedge reflector, (c) 90° wedge reflector.

When Ma_i is between 2.0 and 2.8, the experimental results agree well with the theoretical results, as shown in Fig. 2. The experimental and theoretical results are most consistent when $Ma_i = 2.4$. Ma_i is slightly lower than its theoretical value when the pressure ratio between the driver and driven sections (p_4/p_1) is less than 17. This mismatch could be attributed to the type of shock tube that is employed in the experiment. The theoretical results are based on the one-diaphragm assumption, whereas we adopt a double-diaphragm shock tube in the experiment. When the solenoid valve on the double-diaphragm section opens, the pressure of the double-diaphragm section decreases, leading to a decrease in the pressure difference between the double-diaphragm section and the driven section and an increase in the pressure difference between the driver section and the double-diaphragm section. Therefore, Diaphragm 1, which is shown in Fig. 1(a), will first be ruptured, creating a shock wave that moves into the double-diaphragm section, increasing the pressure and temperature in this section, bringing initial velocity to the local gas. This will enhance the intensity of the final incident shock wave, which will propagate in the driven section after the rupture of Diaphragm 2. However, the error is within the acceptable range considering that Ma_i is lower than 3.0 and p_4/p_1 is lower than 30 in our experiment.

3.2. Two different DDT processes with a planar reflector

Fig. 3 shows the schlieren images of the DDT process under the condition of $Ma_i = 2.2$, and Fig. 4 shows the corresponding pressure and OH* signal records. The time when the incident shock wave enters the schlieren window is set as time zero. This is also suitable for all of the following schlieren images. At $t = 473.3$ μs, a small flame kernel appears at the upper right corner. However, this flame kernel develops at a very low speed, which is still a relatively small flame kernel at $t = 760.0$ μs, turning out to have no significant influence on the whole flow field. Although it cannot be observed from the schlieren images, the PMT signal shows that ignition has already started at approximately $t = 500$ μs, 60 μs delayed from the time that the reflected shock wave passed through the cross-section where PMT and PT4 are located. At $t = 586.7$ μs, a strip flame appears after the reflected shock wave and starts to expand. The hot spot formed at $t = 726.7$ μs is darker than the surroundings in the schlieren image, indicating a higher density gradient at this point. It is formed by the turbulent fluctuations behind the reflected shock wave, which is caused by the pressure perturbation and wrinkling of the turbulent flame. Oran et al.[34] considered that the ignition delay time gradient caused by turbulence is the main

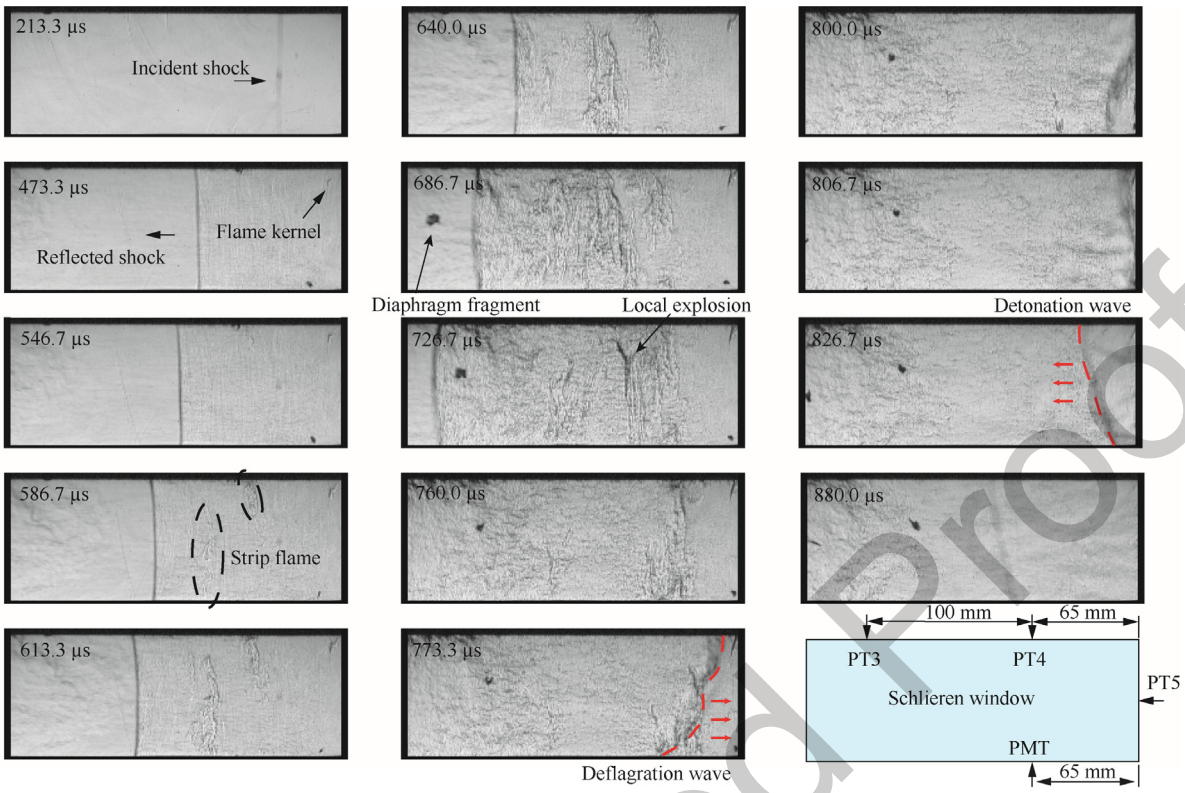

Fig. 3 Schlieren images of DDT process when incident Mach number is 2.2.

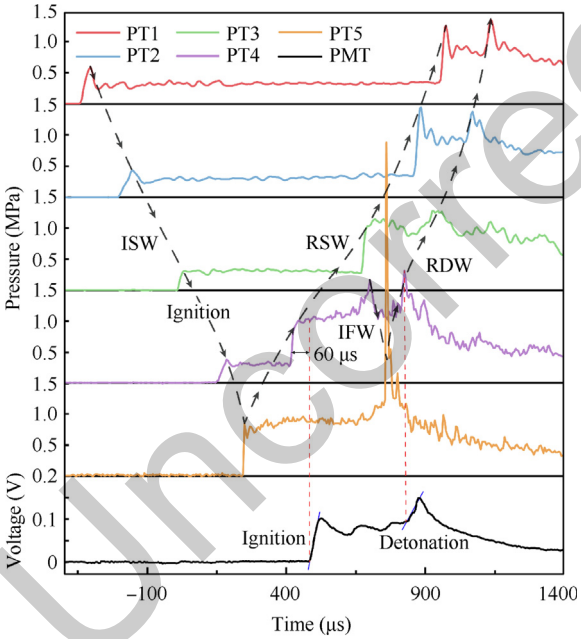

Fig. 4 Pressure and OH* records of planar reflector under condition of $Ma_i = 2.2$.

reason for the autoignition after the reflected shock wave. The important role of flame-turbulence in DDT is also investigated in other researches.[35,36] Owing to the flame-acceleration effect, the initially planar reflected shock wave undergoes a slight outward curvature transformation at $t = 686.7$ μs. Since then, a fast deflagration wave forms from the hot spot, and it propagates toward the planar reflector. The profile of the deflagration wave at $t = 773.3$ μs appears more wrinkled compared to the detonation wave at $t = 826.7$ μs, and no transverse waves are observed after the flame front, indicating that the flame acceleration is still going on. This deflagration wave quickly goes through the DDT process after the collision with the planar reflector, creating a 5.4 MPa peak pressure value at the end wall. Then, it travels as a reflected blast wave toward the driver section, creating a second peak value in PT1–PT4 and PMT. The strong coupling of the flame front and the pressure wave indicates that the reflected blast wave is detonation. The local velocity of the gas after the reflected shock wave can be approximately assumed to be zero, as the diaphragm fragment almost stands still at the same position from 800 μs to 880 μs. Thus, the velocity of the reflected detonation wave is 1008 ± 120.7 m/s, measured from the schlieren images, and it is 77.2% C-J speed ($v_{CJ} = 1306$ m/s).

Fig. 5 depicts another DDT mode where the Mach number of the incident shock wave is 2.3, slightly higher than the situation in Fig. 3. At $t = 280.0$ μs, the reflected shock wave forms, but no combustion wave is observed. The ignition starts at $t = 306.7$ μs, creating a curved deflagration wave after the reflected shock wave. The deflagration wave accelerates and finally catches up with the shock wave at $t = 346.7$ μs. After the coupling of the combustion wave and the shock wave, they form a detonation wave that keeps propagating. The transverse waves after the newly formed combustion wave strongly support that the combustion wave is a detonation wave. More-

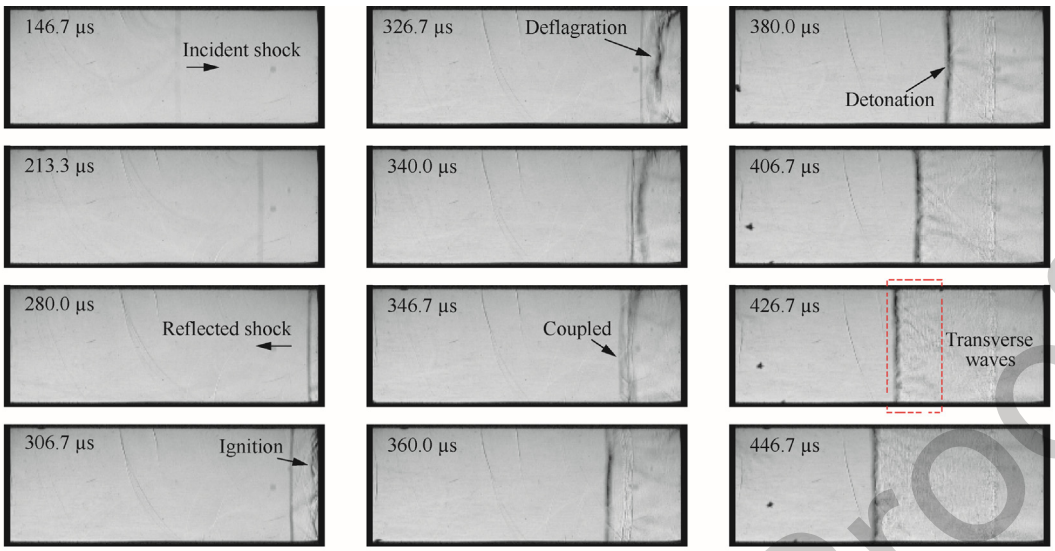

Fig. 5 Schlieren images of DDT process under condition of $Ma_i = 2.3$.

over, the DDT process creates a quasi-stationary density discontinuity at the coupling position because of the different acoustic impedances before and after the shock wave. In general, Fig. 5 shows a typical chemical shock tube ignition process[37] where a combustion wave is formed at the end wall after the reflected shock wave. The subsequent DDT process that this study is focused on is often neglected in traditional ignition delay time measurement experiments.[38]

3.3. Deflagration and detonation in wedge reflectors

Fig. 6 illustrates the deflagration with a 90° wedge reflector under the condition of $Ma_i = 2.0$. Different from the autoignition induced by the planar reflector, the incident shock wave reflects on the wedge, and the reflected shock waves interact with each other, partitioning out several regions. At $t = 320.0$ μs, the reflected bow shock waves encounter each other near the apex of the 90° wedge reflector. The ignition starts from the apex, but the flame is divided by the shock waves into three parts: the upper part, the middle part, and the lower part. At $t = 373.3$ μs, the wave forms after the reflected shock moves at a very low velocity, and the PMT sensor fails to capture the ignition signal during the one-second sampling period. To determine whether it is a flame front, a corresponding cold test is conducted, by replacing the combustible driven gas with a helium-argon mixture that has the same density as the driven gas. The small flow structure at the reflector apex, caused by the complex shock wave interactions[39,40] in the cold test, dissipates rapidly because of the pressure perturbation behind the reflected shock wave. In contrast, the wave near the reflector apex in the combustion case keeps

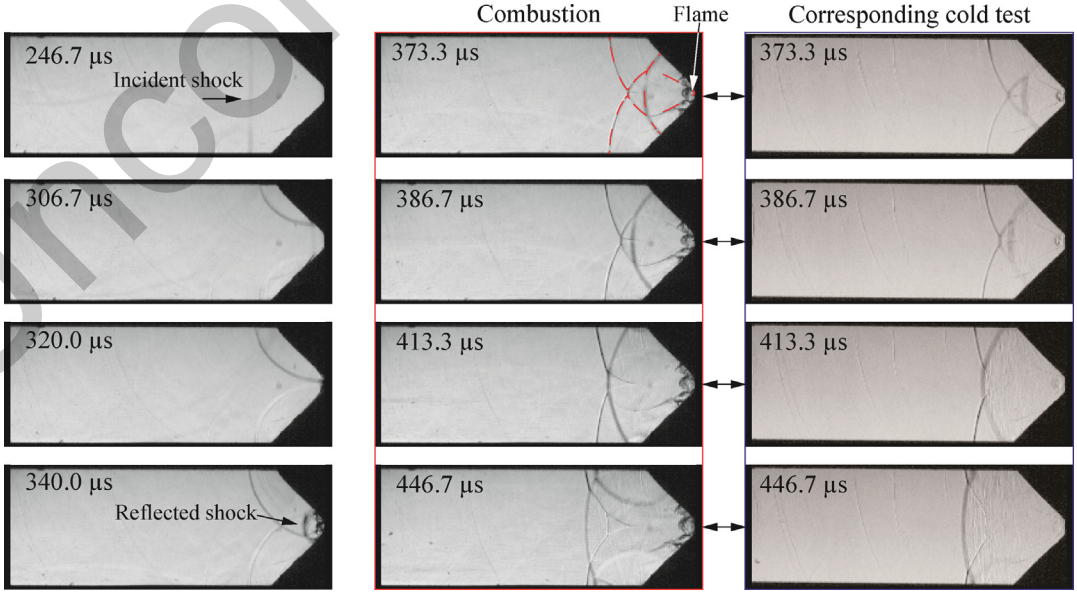

Fig. 6 Schlieren images of deflagration with a 90° wedge reflector and corresponding cold test ($Ma_i = 2.0$).

propagating, indicating that this is a combustion wave. Furthermore, the cold test also shows that the shock wave positions in the combustible case and the cold test are almost identical, which means that the deflagration wave under this condition has no acceleration effect on the reflected shock wave propagation.

The corresponding nonreactive simulation of the cold test in Fig. 6 (t = 340.0 μs) is shown in Fig. 7 for better comprehension. The finite volume OpenFOAM-10[41] package is employed in our simulation. The overall accuracy of the solver utilized here is 2nd order. The computational domain is half of the schlieren window: 200 mm × 36.5 mm, and the minimum mesh size is 10 μm, which is fine enough for nonreactive simulation. A detailed description of the simulation setup can be found in Ref.29. The red line in Fig. 7(a) is the reflected bow shock wave. It is deflected by the reflected shock wave because of the different acoustic impedances before and after the reflected shock wave. A second small bow shock wave (blue) also appears due to the collision between the reflected shock wave and the side wall. Both bow shock wave tails are strongly disturbed by the jet formed from the end wall. The jet is also observed in the schlieren images of nonreactive experiment (Fig. 6, corresponding cold test, t = 373.3 μs). The accumulation line[18] in Fig. 7(b)–(c) shows that the upcoming stream has a turnover here, dividing the local flow field into different parts, which may be the cause of the flame division.

In Fig. 8, the black dashed line represents transverse shock waves, the blue line represents the reflected shock wave, and the red line represents the combustion wave. The schematic diagrams in each frame show the coupling condition of the combustion wave and shock wave. At t = 313.3 μs, the combustion wave has been divided into three parts by the shock waves. The combustion wave couples with the reflected shock wave in Region 1 and Region 3 but decouples in Region 2. It seems that the combustion wave propagates slower in this region. At t = 333.3 μs, the combustion wave develops into a curved shape but almost fully decouples from the reflected shock wave. After 26.7 μs, due to self-acceleration, the combustion wave recouples with the reflected shock wave. At t = 386.7 μs, local decoupling appears again in the middle of the combustion wave, but soon the reflected shock wave recouples with the flame front. The coupling between the combustion wave and the shock wave is highly unsteady in this case.

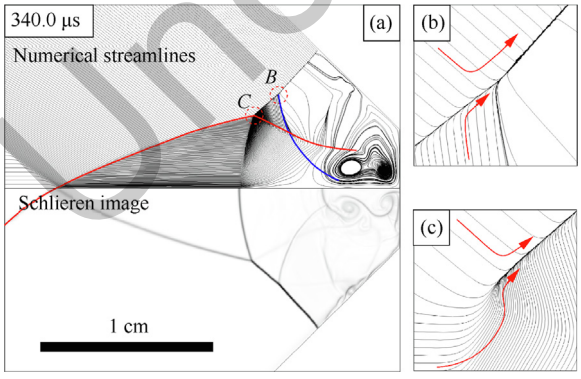

Fig. 7 Nonreactive numerical streamlines and schlieren image with 90° wedge reflector (Ma_i = 2.0): (a) t = 340.0 μs, (b) Enlarged drawing of Point B, (c) Enlarged drawing of Point C.

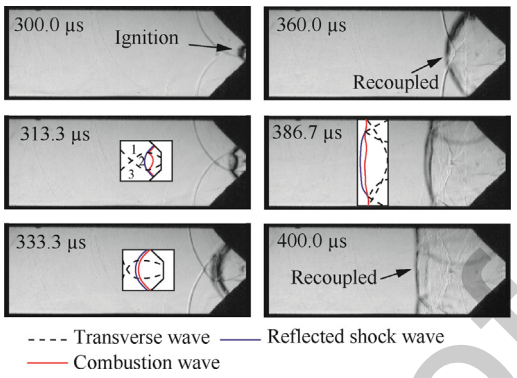

Fig. 8 Local decoupling and recoupling procedure in detonation propagation with a 90° wedge reflector (Ma_i = 2.2).

As a detonation wave propagates from a confined channel to an unconfined space, it undergoes diffraction[42] and has the tendency to fail. Pantow et al.[43] studied the decoupling and recoupling of detonation waves associated with sudden expansion of the tube and found that confined flow conditions after the expansion are responsible for the reinitiation of the decoupled detonation wave. In our research, the wedge-like reflectors act as expansion tubes for the newly formed detonation waves near the reflector apexes, which cause that the detonation waves tend to decouple. Meanwhile, the transverse waves generated from the collision of the detonation wave and the tube wall, as well as the collision of shock waves, strongly support the recoupling of the flame front and the reflected shock wave. As a result, the detonation wave experiences a decoupling and recoupling procedure under the combined effects of the expansion tube and transverse waves.

The schlieren images of detonation with a 60° wedge reflector under the condition of Ma_i = 2.2, which is the same Mach number used in Fig. 8, are shown in Fig. 9. Different from the regular reflection in Fig. 6, the Mach reflection of the incident shock wave makes two triple points collide with each other before the end wall. The detonation wave directly forms after ignition. When the detonation wave propagates through the wedge corner, two strong transverse waves emerge from the corner, which will support the subsequent self-sustained deto-

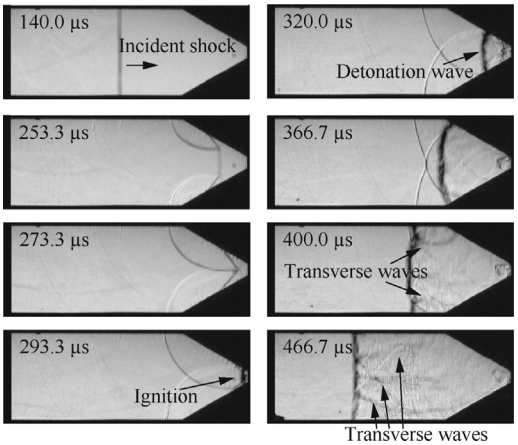

Fig. 9 Schlieren images of detonation with 60° wedge reflector (Ma_i = 2.2).

nation wave propagation. At t = 466.7 μs, three transverse waves are visible after the detonation wave, indicating that the reflected detonation wave is propagating in a stable mode.

3.4. Reflected shock wave velocity and combustion mode identification

Sections 3.2 and 3.3 show several cases, including deflagration, DDT, unsteady detonation, and direct detonation. Fig. 3, Figs. 5–6, and Figs. 8–9 correspond to Shots 1–5 in Fig. 10 and Fig. 11. Fig. 10 depicts the comparison between the relative reflected shock wave velocity and the theoretical reflected shock wave velocity. Due to the coupling of the flame front and shock wave, the speed of the reflected detonation wave will be higher than that of the theoretical nonreactive reflected shock wave. Furthermore, we also confirm that the deflagration wave does not have a significant boost to the leading shock wave. Therefore, if the reflected shock wave velocity v_{re} is close to the theoretical nonreactive shock wave velocity v_{rt}, it can be considered that there is no detonation in the shock tube. However, one exception exists in our experiment, which is Shot 1 in Fig. 10(a). Although v_{re} is lower than v_{rt}, DDT occurs after the reflected shock wave.

Because the reflected detonation wave propagates in the gas with initial velocity v_{2e}, the absolute speed of the detonation wave is $v_{re} + v_{2e}$. However, v_{2e} cannot be obtained from either schlieren images or pressure signals. Section 3.1 shows that the experimental results conform well with the theoretical results. Hence, it is reasonable to use the theoretical velocity of the shocked gas after incident shock wave v_{2t} to substitute v_{2e}. The C-J speed is calculated from the SDToolBox package, which was developed by Shepherd et al.[44], and the package is widely used in detonation simulations. Fig. 11 shows the comparison between the absolute reflected shock wave velocity $v_{re} + v_{2t}$ and C-J velocity v_{CJ}. Four different flame propagation modes are shown in Fig. 11: Deflagration, DDT, unsteady detonation, and direct detonation. The detonation waves formed by DDT only have approximately 75%–86% C-J speed, while the unsteady detonation wave speed is 84.5% C-J speed. It appears that the detonation becomes unstable and experiences a decrease in velocity before ultimately failing. The velocity deficit of the detonation wave is usually found in near-pressure-limit detonation propagation.[45] Strong boundary layer effects, such as small-diameter tubes and rough tube walls,[46,47] can also lead to a decrease in the detonation speed. The onset of phenomena such as single-head spin and the reinitiation procedure found in the aforementioned research all show that the detonation wave is traveling in a relatively unstable state. The decrease proportion of the detonation speed is consistent with our findings.

Compared with the planar reflector, which needs $p_4/p_1 = 22.3$ to form a detonation wave, wedge reflectors only need $p_4/p_1 = 12.5$, nearly reducing half of the initial pressure ratio. The shock wave focusing technique has a great energy-accumulation effect, significantly reducing the pressure ratio required for stable detonation initiation. Although the graphs of the 60° wedge reflector (Fig. 11(b)) and 90° wedge reflector (Fig. 11(c)) have no significant difference, where Shots 4 and 5 have similar reflected shock wave speeds under the same intensity of the incident shock wave (Ma_i = 2.2), the schlieren images (Fig. 8 and Fig. 9) depict that the detonation wave seems to have a more stable propagation mode (strong transverse waves after the detonation wave) in the 60° wedge reflector, which means that the 60° wedge reflector may have a better shock-wave-focusing effect.

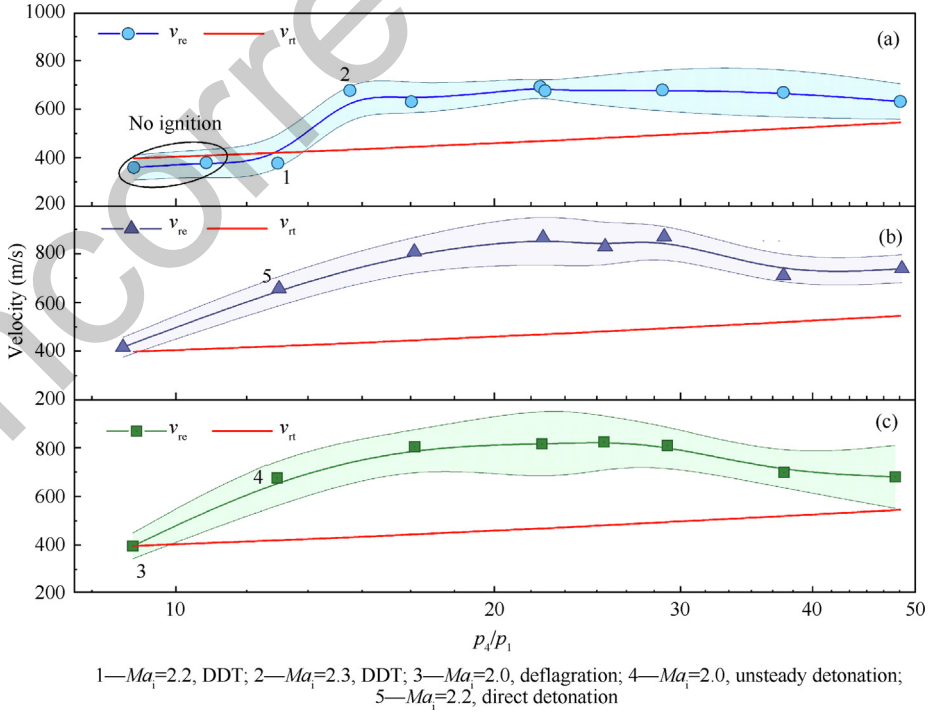

Fig. 10 Comparison between relative reflected shock wave velocity and theoretical reflected shock wave velocity: (a) Planar reflector, (b) 60° wedge reflector, and (c) 90° wedge reflector.

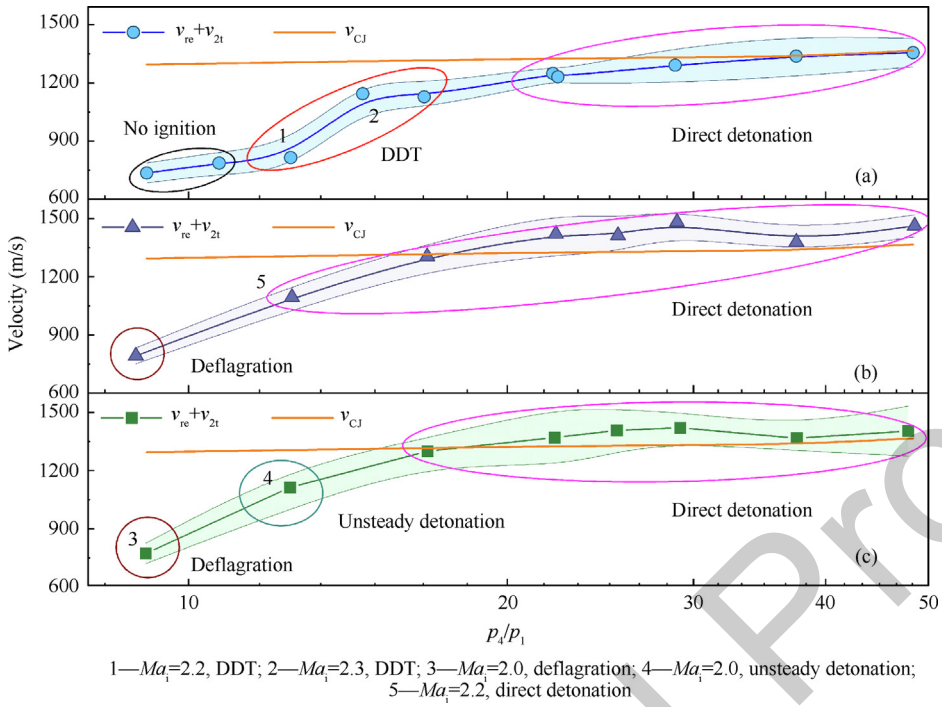

Fig. 11 Comparison between absolute reflected shock wave velocity and C-J velocity: (a) Planar reflector, (b) 60° wedge reflector, and (c) 90° wedge reflector.

4. Conclusions

In this study, the mechanism of deflagration and detonation induced by shock wave focusing in a $H_2/O_2/Ar$ mixture is systematically explored. Schlieren images and the pressure and OH* signals under different conditions are analyzed. The accuracy of the experimental result is validated by comparing it with the theoretical calculation. The speed of the reflected shock waves is utilized to analyze the flame propagation mode. Additional simulation is performed for better understanding. The main conclusions are drawn as follows:

(1) The flame initiated by the collision of the incident shock wave and the end wall generally has four different propagation modes: deflagration, DDT, unsteady detonation and direct detonation. The detonation wave formed in the DDT and unsteady detonation mode seems to only have approximately 75%–85% C-J speed.
(2) In deflagration mode, the velocity of the reflected shock wave is close to the theoretical nonreactive calculation, while in detonation mode, this value is much higher than that of the latter. Therefore, by comparing v_{re} and v_{rt}, one can easily distinguish the deflagration or detonation modes.
(3) Wedge reflectors have a much better energy accumulation effect than planar reflectors. The shock wave focusing technique significantly reduces the initial pressure ratio p_4/p_1 needed for detonation initiation. The 60° wedge reflector may have a better shock-wave-focusing effect than the 90° wedge reflector.

Declaration of Competing Interest

The authors declare that they have no known competing financial interests or personal relationships that could have appeared to influence the work reported in this paper.

Acknowledgment

The authors are grateful for the financial support from the National Natural Science Foundation of China (No. 12272234), the Innovation Program of Shanghai Municipal Education Commission, China (No. 2023KEJI05-75), and the Shanghai Science and Technology Planning Project, China (No. 22190711500).

References

1. Lee JHS. *The detonation phenomenon*. Cambridge: Cambridge University Press; 2008.
2. Ashford S, Emanuel G. Oblique detonation wave engine performance prediction. *J Propul Power* 1996;**12**(2):322–7.
3. Roy GD, Frolov SM, Borisov AA, et al. Pulse detonation propulsion: Challenges, current status, and future perspective. *Prog Energy Combust Sci* 2004;**30**(6):545–672.
4. Jackson SI, Shepherd JE. Toroidal imploding detonation wave initiator for pulse detonation engines. *AIAA J* 2007;**45**(1):257–70.
5. Yu JT, Yao SB, Li JZ, et al. Effects of inlet and secondary flow conditions on the flow field of rotating detonation engines with film cooling. *Int J Hydrog Energy* 2023;**48**(24):9082–94.
6. Xu Z, Dong G, Pan ZH, et al. Standing window of oblique detonation with pathological behaviour. *Chin J Aeronaut* 2021;**34**(5):496–503.

7. Li HB, Li JL, Xiong C, et al. Investigation of hot jet on active control of oblique detonation waves. *Chin J Aeronaut* 2020;**33**(3):861–9.
8. Li R, Xu JL, Lv HY, et al. Numerical investigation of the shock-focusing detonation engines with different nozzle configurations. *Acta Astronaut* 2023;**202**:58–76.
9. Du P, Xue R, Yang Z, et al. Numerical simulation on the shock wave focusing detonation process in the semicircle reflector. *Phys Fluids* 2023;**35**(2) 026107.
10. Zhao XY, Wang JB, Gao LK, et al. Effect of hydrogen concentration distribution on flame acceleration and deflagration-to-detonation transition in staggered obstacle-laden channel. *Phys Fluids* 2023;**35**(1) 016124.
11. Cheng J, Zhang B, Yang ZZ, et al. Investigation of the effect of turbulence induced by double non-reactive gas jet on the deflagration-to-detonation transition. *Aerosp Sci Technol* 2022;**124** 107556.
12. Xiao HH, Oran ES. Shock focusing and detonation initiation at a flame front. *Combust Flame* 2019;**203**:397–406.
13. Peng LY, Dai JA. Effects of staggered opposed hot jets on the initiation and propagation of gaseous detonation in a supersonic combustible inflow. *Phys Fluids* 2023;**35**(1) 014102.
14. Meshkov EE. Reflection of a plane shock wave from a rigid concave wall. *Fluid Dyn* 1970;**5**(4):554–8.
15. Sturtevant B, Kulkarny VA. The focusing of weak shock waves. *J Fluid Mech* 1976;**73**(4):651–71.
16. Duong DQ, Milton BE. The Mach reflection of shock waves in converging, cylindrical channels. *Exp Fluids* 1985;**3**(3):161–8.
17. Izumi K, Aso S, Nishida M. Experimental and computational studies focusing processes of shock waves reflected from parabolic reflectors. *Shock Waves* 1994;**3**(3):213–22.
18. Lodato G, Vervisch L, Clavin P. Direct numerical simulation of shock wavy-wall interaction: analysis of cellular shock structures and flow patterns. *J Fluid Mech* 2016;**789**:221–58.
19. Bond CL, Hill DJ, Meiron D, et al. Shock focusing in a planar convergent geometry: experiment and simulation. *J Fluid Mech* 2009;**641**:297–333.
20. Eliasson V, Kjellander M, Apazidis N. Regular versus Mach reflection for converging polygonal shocks. *Shock Waves* 2007;**17**(1):43–50.
21. Dimotakis PE, Samtaney R. Planar shock cylindrical focusing by a perfect-gas lens. *Phys Fluids* 2006;**18**(3) 031705.
22. Zhai ZG, Liu CL, Qin FH, et al. Generation of cylindrical converging shock waves based on shock dynamics theory. *Phys Fluids* 2010;**22**(4) 041701.
23. Luo XS, Si T, Yang JM, et al. A cylindrical converging shock tube for shock-interface studies. *Rev Sci Instrum* 2014;**85**(1) 015107.
24. Liverts M, Apazidis N. Limiting temperatures of spherical shock wave implosion. *Phys Rev Lett* 2016;**116** 014501.
25. Chan CK. Collision of a shock wave with obstacles in a combustible mixture. *Combust Flame* 1995;**100**(1–2):341–8.
26. Gelfand BE, Khomik SV, Bartenev AM, et al. Detonation and deflagration initiation at the focusing of shock waves in combustible gaseous mixture. *Shock Waves* 2000;**10**(3):197–204.
27. Bartenev AM, Khomik SV, Gelfand BE, et al. Effect of reflection type on detonation initiation at shock-wave focusing. *Shock Waves* 2000;**10**(3):205–15.
28. Zhang B, Li YC, Liu H. Ignition behavior and the onset of quasi-detonation in methane-oxygen using different end wall reflectors. *Aerosp Sci Technol* 2021;**116** 106873.
29. Zhang B, Li YC, Liu H. Analysis of the ignition induced by shock wave focusing equipped with conical and hemispherical reflectors. *Combust Flame* 2022;**236** 111763.
30. Smirnov NN, Penyazkov OG, Sevrouk KL, et al. Detonation onset following shock wave focusing. *Acta Astronaut* 2017;**135**:114–30.
31. Smirnov NN, Penyazkov OG, Sevrouk KL, et al. Onset of detonation in hydrogen-air mixtures due to shock wave reflection inside a combustion chamber. *Acta Astronaut* 2018;**149**:77–92.
32. Li YC, Zhang B. Visualization of ignition modes in methane-based mixture induced by shock wave focusing. *Combust Flame* 2023;**247** 112491.
33. Yang ZZ, Zhang B. Numerical and experimental analysis of detonation induced by shock wave focusing. *Combust Flame* 2023;**251** 112691.
34. Oran ES, Young TR, Boris JP, et al. Weak and strong ignition. I. Numerical simulations of shock tube experiments. *Combust Flame* 1982;**48**:135–48.
35. Zhao WD, Liang JH, Deiterding R, et al. Flame–turbulence interactions during flame acceleration using solid and fluid obstacles. *Phys Fluids* 2022;**34**(10) 106106.
36. Peng H, Huang Y, Deiterding R, et al. Effects of jet in crossflow on flame acceleration and deflagration to detonation transition in methane-oxygen mixture. *Combust Flame* 2018;**198**:69–80.
37. Brown CJ, Thomas GO. Experimental studies of shock-induced ignition and transition to detonation in ethylene and propane mixtures. *Combust Flame* 1999;**117**(4):861–70.
38. Petersen EL, Davidson DF, Hanson RK. Ignition delay times of ram accelerator CH/O/diluent mixtures. *J Propuls Power* 1999;**15**(1):82–91.
39. Inoue O, Takahashi N, Takayama K. Shock wave focusing in a log-spiral duct. *AIAA J* 1993;**31**(6):1150–2.
40. Taieb D, Ribert G, Hadjadj A. Numerical simulations of shock focusing over concave surfaces. *AIAA J* 2010;**48**(8):1739–47.
41. Jasak H, Jemcov A, Tukovic Z. OpenFOAM: A C++ library for complex physics simulations. *International workshop on coupled methods in numerical dynamics*. 2007. p. 1–20.
42. Gallier S, Le Palud F, Pintgen F, et al. Detonation wave diffraction in H_2-O_2-Ar mixtures. *Proc Combust Inst* 2017;**36**(2):2781–9.
43. Pantow EG, Fischer M, Kratzel T. Decoupling and recoupling of detonation waves associated with sudden expansion. *Shock Waves* 1996;**6**(3):131–7.
44. Browne S, Ziegler J, Shepherd JE. Numerical solution methods for shock and detonation jump conditions. 2008. Report No.: FM2006.006.
45. Lee JHS, Jesuthasan A, Ng HD. Near limit behavior of the detonation velocity. *Proc Combust Inst* 2013;**34**(2):1957–63.
46. Teodorczyk A, Lee JHS, Knystautas R. Propagation mechanism of quasi-detonations. *Symp Int Combust* 1989;**22**(1):1723–31.
47. Zhang B. The influence of wall roughness on detonation limits in hydrogen-oxygen mixture. *Combust Flame* 2016;**169**:333–9.

Please cite this article in press as: YANG Z et al. Deflagration and detonation induced by shock wave focusing at different Mach numbers, *Chin J Aeronaut* (2023), https://doi.org/10.1016/j.cja.2023.06.029